The Structure of Blood–tumor Barrier and Distribution of Chemotherapeutic Drugs in Non-small Cell Lung Cancer Brain Metastases

Ling-yun Ye (yelingyun0712@126.com)
Tongji University Affiliated Shanghai Pulmonary Hospital https://orcid.org/0000-0003-4259-9288
Li-xiang Sun
The Affiliated Hospital of Xuzhou Medical University: Xuzhou Medical University Affiliated Hospital
Xiu-hua Zhong
Nanjing Medical University Affiliated Wuxi People's Hospital: Wuxi People's Hospital
Xue-song Chen
Jiangsu Province Hospital and Nanjing Medical University First Affiliated Hospital
Song Hu
Changzhou First People's Hospital
Rong-rong Xu
Southeast University Zhongda Hospital
Xiao-ning Zeng
Jiangsu Province Hospital and Nanjing Medical University First Affiliated Hospital
Wei-ping Xie
Jiangsu Province Hospital and Nanjing Medical University First Affiliated Hospital
Hui Kong
Jiangsu Province Hospital and Nanjing Medical University First Affiliated Hospital

Research Article

Keywords: non-small cell lung cancer, brain metastasis, blood-brain barrier, blood-tumor barrier, chemotherapeutic drugs

Posted Date: July 30th, 2021

DOI: https://doi.org/10.21203/rs.3.rs-719723/v1

Abstract

Background: Brain metastasis is an important cause increasing the mortality of non-small cell lung cancer (NSCLC) patients. In brain metastasis, blood-brain barrier (BBB) is frequently impaired, while blood-tumor barrier (BTB) formed and leading to poor effects of chemotherapy. However, the characteristics of BTB and the impacts of BTB on chemotherapeutic drug delivery remain unclear. The present study investigated the structure of BTB, as well as the distribution of routine clinical chemotherapeutic drugs in both brain and peripheral tumors.

Methods: Bioluminescent image was used to confirm the formation of brain metastases of transplanted lung cancer Lewis cells in mice. The permeability of BBB and BTB was measured by fluorescent tracers of evans blue and fluorescein sodium. Transmission electron microscopy (TEM), immunohistochemistry and immunofluorescence were performed to analyze structural differences between BBB and BTB. The content of chemotherapeutic drugs (gemcitabine, paclitaxel and pemetrexed) in tissues was assayed by liquid chromatography with tandem mass spectrometry (LC-MS/MS).

Results: Brain metastasis exhibited increased BTB permeability compared with normal BBB detected by fluorescence tracers. TEM showed abnormal blood vessels, damaged endothelial cells, thick basement membranes, impaired intercellular endothelial tight junctions, as well as increased fenestrae and pinocytotic vesicles in metastatic lesions. Immunohistochemistry and immunofluorescence revealed that astrocytes were distributed surrounded the blood vessels both in normal brain and the tumor border, but no astrocytes were found in the inner metastatic lesions. By LC-MS/MS analysis, gemcitabine and paclitaxel showed higher permeability in brain metastatic lesions.

Conclusions: Brain metastases of lung cancer disrupted the structure of BBB, and this disruption was heterogeneous. Chemotherapeutic drugs can cross the BTB of brain metastases of lung cancer but have difficulty crossing the normal BBB. The permeability of chemotherapeutic agents is related to their molecular weight and liposolubility.

Introduction

Lung cancer is one of the most common malignant tumors and remains the leading cause of cancer-related lethality worldwide (1, 2). Non-small cell lung cancer (NSCLC), as the main histological type of lung cancer, accounts for 80% of all cases. Advanced imaging technologies improved treatment approaches, and earlier detection of clinically silent lesions have prolonged the survival of patients with lung cancer (3). However, one unfortunate consequence of prolonged survival is that patients may eventually suffer from tumor metastases, especially brain metastasis.

Most metastatic brain tumors, accounting for about 45%, originate from lung cancer (4, 5). Currently, patients with brain metastases are usually considered to be terminal with poor prognosis. Approximately 40–50% of patients diagnosed with NSCLC are estimated to develop brain metastasis during the course of the disease (6–8). The overall survival for the patients is 2 months with palliative treatment; even with

radiation therapy, the survival remains poor with median survival time of 7.6 months (6–8). Thus, effective treatments of NSCLC with brain metastases are considered to be critical for improving the prognosis of advanced lung cancer patients.

The locations of brain metastases are related to blood flow and tissue volume, with approximately 80% detected in the cerebral hemispheres, 15% in the cerebellum, and 5% in the brainstem (3). Despite of many advances that have been made in the treatment of NSCLC, including chemotherapy, surgery, targeted therapy, stereotactic radiosurgery (SRS), and whole-brain radiotherapy (WBRT), the prognosis of patients with brain metastases is still dismal (9–11). Systemic chemotherapies have little success in the treatment of brain metastases which is considered to be at least partially due to the presence of blood-brain barrier (BBB) (12–13). The BBB is formed by specialized endothelial cells, pericytes and astrocytic perivascular endfeet. The adjacent cells are tightly connected to each other via intercellular junctions, preventing most molecules to pass through endothelial cells. In addition, the constituents of the BBB express high levels of active efflux drug transporters, such as the P-glycoprotein and multidrug resistance proteins (14). Together, these factors curb the accessibility and delivery of therapeutic agents to the brain parenchyma. Some previous studies suggested that the BBB is disrupted in brain metastases, creating a blood–tumor barrier (BTB) (15). It has been debated for several years whether BTB overrides BBB in metastasis. In addition, the impacts of BTB on chemotherapeutic drugs transport remains unclear in brain metastases treatments (16–17).

The present study aimed to investigate the structure and characteristics of the BTB in brain metastases of NSCLC. Using stereotactic intracranial injection of tumor cells in mice to establish brain metastasis model of lung cancer, the structural differences between healthy BBB and barrier of brain metastases were investigated. To provide the basis for choosing clinical chemotherapeutic drugs and optimizing treatment, we explored the distribution of routine chemotherapeutic drugs for NSCLC in brain metastases.

Materials And Methods

Cell culture and labeling

Lewis cells were purchased from the Institute of Biochemistry and Cell Biology of the Chinese Academy of Sciences (Shanghai, China). The cells were propagated in RPMI 1640 medium (Gibco BRL) supplemented with 10% fetal bovine serum (ScienCell, USA), 100 U/ml penicillin and 100 U/ml streptomycin at 37 °C in a 5% CO_2 humidified atmosphere. Luc-lentivirus was purchased from Genechem Co., Ltd. The cells were seeded on culture plates, and a moderate amount of Luc-lentivirus was added to the plate according to the instructions. Clones stably expressing luciferase were selected with neomycin.

Animal experiments

Athymic nu/nu mice (7 to 8 weeks of age, 21-25 g each) were purchased from Shanghai, China. The mice were maintained under controlled conditions (room temperature and 12-h light/dark cycle) and had access to standard food and water ad libitum. All experiments were conducted according to the

guidelines of the National Institutes of Health. The experimental procedures were approved by the Institutional Animal Care and Use Committee of Nanjing Medical University.

Stereotactic intracranial injection of tumor cells

Mice were anesthetized with 4% chloral hydrate and placed in a stereotactic frame (RWD Life Science, Shenzhen, China). A middle incision was made, followed by a 0.5-mm burr hole that was 2 mm lateral and 2 mm posterior to the bregma. Then, 4 μl of cell suspension containing approximately 5×10^4 Lewis cells was slowly injected intracranially using a 10 μl microinjector syringe at 3 mm below the skull surface over a period of 3 min. The needle was then removed over a 3-min period, and the incision was closed. The mice were monitored until regaining consciousness and were returned to their cages.

In vivo bioluminescent imaging

Mice were i.p. injected with 150 mg/kg D-luciferin potassium salt (15 mg/ml in phosphate-buffered saline (PBS), Shanghai Sciencelight Biology Science & Technology Co., Ltd.) and anesthetized with isoflurane (2-3%). Ten minutes after injection, images were acquired using an IVIS 200 system. The bioluminescent signal was measured as photons per second per square centimeter in regions of interest using Living Image software.

Intravascular injection and detection of fluorescence tracers

A solution of 2% Evans blue (EB, 4 ml/kg, Sigma, USA) was injected into each animal via the femoral vein and circulated for 30 min. After 25 min of EB circulation, fluorescein sodium (F-Na, 300 mg/kg, Sigma, USA) was administered intravenously to circulate for 5 min. Anesthetized mice were perfused with saline to wash out excess fluorescence tracers, and then euthanized by cervical dislocation, after which the brains were quickly removed and embedded in optimum cutting temperature (OCT, Sakura, USA) cryostat-embedding compound. Next, the brains were frozen in liquid nitrogen and sliced into 40-μm thick sections at -19 °C. The penetration of fluorescence tracers through the BBB was further assessed by fluorescence microscopy (Leica, Germany).

Hematoxylin and eosin staining

To confirm the presence of intracranial xenografts, anesthetized mice euthanized by cervical dislocation and whole brains of mice were removed and fixed in a neutral-buffered 10% formaldehyde solution overnight. Then, the brains were embedded in paraffin, sectioned into 4 μm slices and stained with hematoxylin and eosin (H&E).

Transmission electron microscopy analysis

Mice were anesthetized by intraperitoneal injection of pentobarbital sodium (70 mg/kg) and perfused through the left ventricle with 100 ml saline followed by 100 ml 4% paraformaldehyde. The brains were removed, fixed in glutaraldehyde, dehydrated in acetone, embedded with epoxy resin, and sliced into

ultrathin sections. Then, the sections were observed under a transmission electron microscope (JEM-1010, Japan).

Immunohistochemistry (IHC) methods

Mice were euthanized as mentioned above, the brains were removed for alcohol dehydration and paraffin embedding. Paraffin-embedded tissue slices were deparaffinized in xylene, rehydrated in graded ethanol, and rinsed with PBS. Then, the slices were placed in a repair box filled with EDTA antigen repair buffer (pH 8.0) and incubated with BSA. The sections were then incubated overnight at 4 °C with polyclonal antibodies against GFAP (Abcam, USA) and CD31 (Santa Cruz, USA). After washing, the slides were incubated with secondary antibody (Life, USA) for 1 h at room temperature. Finally, the slides were visualized by incubation with 3, 3'-diaminobenzidine (DAB) and counterstained with hematoxylin (37%).

Immunofluorescence (IF) methods

The procedure was similar to that used for IHC analysis. Briefly, paraffin-embedded tissue slices were deparaffinized in xylene, rehydrated in graded ethanol, rinsed with PBS, and incubated with primary and secondary antibodies. Then, the slices were incubated with Hoechst staining buffer for 30 min at room temperature and analyzed via fluorescence microscopy (Leica, Germany).

Drug treatments

The chemotherapeutic drugs were administered 7 days after Lewis cells implantation in mice. All drugs were prepared immediately before use and were given at a dose volume of 10 ml/kg via tail vein. Paclitaxel was administered as an alcohol solution of Cremophor (Cremophor dose, 1.2 ml/kg), and gemcitabine and pemetrexed were given as a water solution. The drugs were administered at the dose level of 30 mg/kg to mice bearing tumors (n = 5 per group).

LC-MS/MS analysis

As mentioned above, the mice in each group were anesthetized and then euthanized by cervical dislocation. Blood, brain tumors, healthy brain tissues and subcutaneous tumors were rapidly obtained at 15 min, 30 min, 1 h, 2 h and 4 h after injection of the chemotherapeutic drugs for liquid chromatography-mass spectrometry analysis. Liquid chromatography with tandem mass spectrometry (LC-MS/MS) was performed using an Agilent 1290 series HPLC system (Agilent Technologies, Palo Alto, CA, USA) coupled to an Agilent 6460 triple-quadrupole mass spectrometer (Agilent Technologies, Palo Alto, CA, USA) equipped with electrospray ionization (ESI). Analytes were separated with matrices using a Waters Symmetry 300 C18 column (2.1*100 mm, 3.5 μm; Torrance, CA, USA) maintained at 20 °C. The mobile phase of the pemetrexed group samples was 1% formic acid and 0.5% methanol, and the flow rate was 0.3 ml/min. The mobile phases of the gemcitabine and paclitaxel group samples were 10 mM ammonium acetate in aqueous solution and acetonitrile, and the flow rates were 0.4 ml/min and 0.45 ml/min, respectively. A triple-quadrupole mass spectrometer was used to detect the analytes by ESI in the positive mode. MRM mode was used to detect the product ions. The MS parameters were as follows:

pemetrexed group samples: Gas Temp: 350 °C, Gas Flow: 10 l/min, Nebulizer: 40 psi, Sheath Gas Heater: 350 °C, Sheath Gas Flow: 9 l/min, and Capillary: 4000; gemcitabine group samples: Gas Temp: 350 °C, Gas Flow: 8 l/min, Nebulizer: 40 psi, and Capillary: 4000; and paclitaxel group samples: Gas Temp: 350 °C, Gas Flow: 10 l/min, Nebulizer: 40 psi, Sheath Gas Heater: 350 °C, Sheath Gas Flow: 8 l/min, and Capillary: 3500. The column effluent was monitored at the following precursor–product ion transitions: m/z 428.1 → 163.1 for pemetrexed, m/z 641.1→112.0 for gemcitabine and m/z 876.3 → 308.0 for paclitaxel, with a dwell time of 100 ms for each ion transition. The total run time was 6 min for pemetrexed, 8 min for gemcitabine and 5 min for paclitaxel.

Statistical analysis

All experiments were performed at least three times. Data are expressed as the mean ± SEM. All statistical analyses were performed using one-way analysis of variance (ANOVA) followed by a Dunnett post hoc test with Prism 6.00 software (GraphPad Software, San Diego, CA, USA) and SPSS version 20 (SPSS Inc., Chicago, IL, USA). $P < 0.05$ was considered to indicate significant differences.

Results

Tumor development after stereotactic intracranial injection of tumor cells

Lewis cells were transfected with Luc reporter gene. Cells with fluorescence intensity above 10^2 p/sec/cm^2/sr were considered to be successfully transfected and were used in subsequent experiments (Fig. 1). From the 7th day after injection, some mice exhibited dysactivity, seizures and convulsions. As shown in Fig. 2, the volume of brain metastases increased gradually after implantation of Lewis cells measured by fluorescence intensity and H&E staining.

Btb Permeability

As shown in Fig. 3A and B, the fluorescence of F-Na, the low molecular weight tracer, was observed in brain metastases at day 4; while both the high and low molecular weight tracers (EB and F-Na) penetrated into the metastases at day 6. However, no fluorescence was observed in normal area of the brain. The results showed that the permeability of BTB in metastatic lesions was increased compared with BBB in normal area. Additionally, the permeability of BTB was increased with the time.

Structural Differences Between Bbb And Btb

As shown in TEM, the ultrastructure of the BBB in brain metastases was abnormal. Figure 4A showed the normal BBB, while Fig. 4B and 4C were the BBB of brain metastases. As shown in Fig. 4B, the tight junctions between endothelial cells were opened. In Fig. 4C, thickened basement membranes, increased

fenestrae, and pinocytotic vesicles were found in the BBB of brain metastases. The IHC and IF staining showed that astrocytes were distributed surrounded the blood vessels both in normal brain and at the tumor border, but no astrocytes were found in brain metastases (Fig. 5).

Effects Of Tumor Size On Bbb Structure

Figure 6 shows that most astrocytes were recruited at the border of brain metastases, while there are scattered astrocytes migrating around the blood vessels within the relatively small tumor foci after 4 days of implantation. As the tumor grows (after 6 days of implantation), the numbers of astrocytes within the tumors decreased significantly and disappeared ultimately. No astrocytes were observed around the blood vessels, but they were still visible at the tumor boundary.

Distribution Of Chemotherapeutic Drugs

By LC-MS/MS analysis, the concentrations of gemcitabine, paclitaxel and pemetrexed in subcutaneous tumors were highest (Fig. 7A and C). Besides, all agents had higher concentrations in the brain metastases than in the normal brain, indicating that they could cross the BTB but had difficulty penetrating the normal BBB (Fig. 7A and B). In addition, the concentrations of gemcitabine and pemetrexed in all tissues were decreased gradually after injection because of the short half-life, while the half-life of paclitaxel was long, so the concentrations of paclitaxel in plasma, subcutaneous tumor and brain tumor were increased gradually after injection (Fig. 7A). Moreover, compared with paclitaxel and pemetrexed, gemcitabine had the highest concentration in brain tumor, suggesting that gemcitabine was more likely to penetrate into brain metastases (Fig. 7D).

Discussion

Lung cancer remains the leading cause of cancer-related mortality worldwide (18). The propensity for metastasis to the central nervous system (CNS) is a major problem in the management of lung cancer patients. It usually represents a poor prognosis since most patients are at the end stage of disease progression (19). Thus, it is important to understand the brain metastasis in NSCLC. The dismal prognosis of lung cancer metastasis in the brain involves in many mechanisms. Chemotherapeutic drug resistance is the main cause of death in patients with brain metastasis. Recently, increasing evidence have shown that when brain metastases occur, the formation of BTB replaces the normal BBB, exhibiting different structural and functional characteristics. The protective effects of the BTB are significantly weakened (20). This study focused on investigating the relationship between the BTB and the delivery and efficacy of chemotherapeutic agents.

A mice model of NSCLC metastasis in brain was established to fully elucidate the structural differences between BBB and BTB, as well as the effects of BBB and BTB on chemotherapy. The results showed that the structures of the barriers in metastases changed substantially, and blood vessels at the invasive edge

and center of the tumors were abnormal. Compared with those in healthy brain tissue, the endothelial cells in the metastatic lesions were damaged, the basement membranes were thicker, the endothelial tight junctions were open, the numbers of fenestrae and pinocytotic vesicles were increased, and astrocyte encapsulation was absent around blood vessels. However, at the edge of the tumor, the barrier structure was intact, indicating that such damage was heterogeneous, and these structural differences were related to tumor size (21). Although the BTB is more permeable than normal BBB, it still impedes the entry of antitumor drugs into brain tissues.

Under physiological conditions, BBB is regarded as a neurovascular unit, composing of tightly connected endothelial cells and maintained by crosstalk with astrocytes and pericytes. BBB plays a vital role in restricting the passage of circulating macromolecules into brain parenchyma (22). The BBB and the lack of a lymphatic system are responsible for maintaining the brain as an immunologically privileged site. In addition, BBB protects the brain against the entry of microorganisms and most drugs, maintaining the stability of the brain environment (23). Astrocytes, as important components of the BBB, participate in neurogenesis, neuronal proliferation, migration, differentiation, neuronal signal transduction, nutrient transport, secretion of neurotrophic factors, and immune activation to prevent the invasion of foreign substances. Therefore, astrocytes have been considered as key orchestrators for regulating BBB integrity and permeability (24, 25). Due to the lack of lymphatic system, astrocytes also serve as immune modulator preventing the invasion of microbial and the entry of drugs (23, 26). In addition, the transport proteins distributed on the membrane of brain capillary endothelial cells also play important roles in maintaining the selective permeability of the BBB (27). P-gp, an ATP-dependent phosphoglycoprotein, is highly expressed in endothelial cells of BBB, and this high expression of P-gp is found to be an important mechanism of multidrug resistance (MDR) in tumors. Animal studies have shown that P-gp inhibitors can increase the concentration of chemotherapeutic drugs in brain metastases, improving the chemotherapeutic efficiency of brain metastases from lung cancer (28).

The BBB permeability reveals a notable size-effect of brain metastases. Previous studies have shown that the BBB permeability of brain metastases larger than 0.5 mm in diameter is significantly increased compared to that of scattered infiltrating and smaller lesions. With an increase in tumor volume, ischemic necrosis may occur in the center of the lesion, promoting the synthesis and secretion of vascular endothelial growth factor (VEGF) (29, 30). VEGF can increase BBB permeability via destroying VE-cadherin-β-catenin junction complex (31). In addition, the up-regulation in endothelial cell vesicle density through up-regulation of pit protein expression is another important mechanism for increased BBB permeability (32). Despite of much effort, more in-depth studies are still needed to further understand these complex mechanisms. Our study showed that the BBB was disrupted in brain metastasis of lung cancer, and the permeability was increased as the tumor growth. There is a significant structural difference observed between the BTB and normal BBB.

Current chemotherapy generally has limited efficacy in eradicating metastatic lesions. The infiltration of chemotherapeutic drugs into the brain is not only related to the BBB structure, but also to the molecular size, charge state, liposolubility and binding power with plasma proteins of the drug. Drugs with a low

molecular weight, low plasma protein binding rate and high liposolubility can easily penetrate the BBB, while water-soluble drugs with high molecular weight and polarity have difficulty in penetrating the BBB. Among the three chemotherapeutic drugs in our study, gemcitabine had the smallest molecular weight, followed by pemetrexed, paclitaxel had the largest molecular weight, but only paclitaxel was lipophilic. We found that gemcitabine had the highest concentration in brain metastases, probably because of its small molecular weight. The molecular weight of paclitaxel was larger than that of pemetrexed, but its concentration in brain metastases was slightly higher than that of pemetrexed, which may be due to its high liposolubility, suggesting that the permeability of chemotherapeutic drugs in brain metastases is closely related to their molecular weight and liposolubility.

Conclusion

The present work demonstrated that NSCLC metastases in the brain disrupt the BBB leading to the formation of BTB, and this disruption was not homogeneous. The permeability of the impaired barrier was associated with the tumor size. Chemotherapeutic agents can pass through the BTB of metastatic lesions but have difficulty in penetrating the normal BBB. The permeability of chemotherapeutic agents is related to their molecular weight and liposolubility. Understanding the structural differences between BBB and BTB shed light on improving chemotherapeutic drug transport for treating brain metastases in NSCLC.

Abbreviations

non-small cell lung cancer (NSCLC), blood-brain barrier (BBB), blood-tumor barrier (BTB), Transmission electron microscopy (TEM), stereotactic radiosurgery (SRS), whole-brain radiotherapy (WBRT), Evans blue (EB), fluorescein sodium (F-Na), hematoxylin and eosin (H&E), Immunohistochemistry (IHC), Immunofluorescence (IF), diaminobenzidine (DAB), electrospray ionization (ESI), Liquid chromatography with tandem mass spectrometry (LC-MS/MS), one-way analysis of variance (ANOVA), central nervous system (CNS), multidrug resistance (MDR), vascular endothelial growth factor (VEGF).

Declarations

Acknowledgments

None.

Author Contributions

Ling-yun Ye, Li-xiang Sun performed the establishment of brain metastasis model of lung cancer and the immunohistochemistry and immunofluorescence. Xue-song Chen, Song Hu and Rong-rong Xu participated in the permeability experiment. Ling-yun Ye and Li-xiang Sun performed the TEM and the LC-MS/MS analysis. Xiao-ning Zeng helped to guide the experimental operation. Ling-yun Ye and Xiu-hua

Zhong drafted the manuscript. Wei-ping Xie and Hui Kong participated in the design of the study and the revision of the manuscript. All authors read and approved the final manuscript.

Funding

This study was supported by the National Technological Special Project for “Significant New Drugs Development” (2011ZX09302-003-02), Jiangsu Province Major Scientific and Technological Special Project (No. BM2011017), a Project Funded by the Priority Academic Program Development of Jiangsu Higher Education Institutions (PAPD) and the "Young eagle" program of young doctors of Shanghai anti-cancer association (SACA-CY19B05).

Data availability statement

The data used in the current study are available from the corresponding author on reasonable request.

Availability of data and materials

The data supporting the conclusions of this study are included within the article.

Ethics approval and consent to participate

The present study was approved by the Institutional Animal Care and Use Committee of Nanjing Medical University.

Consent for publication

Not applicable.

Competing interests

The authors declare that there have no competing interests.

References

1. Siegel R, et al. Cancer statistics, 2011. CA: A Cancer Journal for Clinicians. 2011; 61(4):212-36.
2. Li G. Meta-analysis of GSTM1 null genotype and lung cancer risk in Asians. Medical Science Monitor. 2014;20:1239-45.
3. Eichler AF, et al. The biology of brain metastases—translation to new therapies. Nature Reviews Clinical Oncology. 2011;8(6):344-56.
4. Sørensen JB, et al. Brain metastases in adenocarcinoma of the lung: frequency, risk groups, and prognosis. Journal of Clinical Oncology. 1988;6(9):1474-80.
5. Lagerwaard F, et al. Identification of prognostic factors in patients with brain metastases: a review of 1292 patients. International Journal of Radiation Oncology*Biology*Physics. 1999;43(4):795-803.

6. Pfannschmidt J, Dienemann H. Surgical treatment of oligometastatic non-small cell lung cancer. Lung Cancer. 2010;69(3):251-8.
7. Villaruz LC, et al. Management of Non-Small Cell Lung Cancer with Oligometastasis. Current Oncology Reports. 2012;14(4):333-41.
8. Yamanaka. Medical management of brain metastases from lung cancer (Review). Oncology Reports. 2009;22(06).
9. Steeg PS, et al. Brain metastases as preventive and therapeutic targets. Nature Reviews Cancer. 2011;11(5):352-63.
10. Oberhoff C, et al. Topotecan Chemotherapy in Patients with Breast Cancer and Brain Metastases: Results of a Pilot Study. Oncology Research and Treatment. 2001;24(3):256-60.
11. Krop IE, et al. Trastuzumab emtansine (T-DM1) versus lapatinib plus capecitabine in patients with HER2-positive metastatic breast cancer and central nervous system metastases: a retrospective, exploratory analysis in EMILIA. Annals of Oncology. 2015;26(1):113-9.
12. Lin NU, et al. Multicenter Phase II Study of Lapatinib in Patients with Brain Metastases from HER2-Positive Breast Cancer. Clinical Cancer Research. 2009;15(4):1452-9.
13. Deeken JF, Löscher W. The Blood-Brain Barrier and Cancer: Transporters, Treatment, and Trojan Horses. Clinical Cancer Research. 2007;13(6):1663-74.
14. Ohtsuki S, Terasaki T. Contribution of Carrier-Mediated Transport Systems to the Blood–Brain Barrier as a Supporting and Protecting Interface for the Brain; Importance for CNS Drug Discovery and Development. Pharmaceutical Research. 2007;24(9):1745-58.
15. Gerstner ER, Fine RL. Increased Permeability of the Blood-Brain Barrier to Chemotherapy in Metastatic Brain Tumors: Establishing a Treatment Paradigm. Journal of Clinical Oncology. 2007;25(16):2306-12.
16. de Vries NA, et al. Blood–brain barrier and chemotherapeutic treatment of brain tumors. Expert Review of Neurotherapeutics. 2006;6(8):1199-209.
17. Donelli MG, et al. Do anticancer agents reach the tumor target in the human brain? Cancer Chemotherapy and Pharmacology. 1992;30(4):251-60.
18. Whitsett TG, et al. Molecular determinants of lung cancer metastasis to the central nervous system. Translational lung cancer research. 2013;2(4):273-83.
19. Gállego Pérez-Larraya J, Hildebrand J. Brain metastases. Handb Clin Neurol. 2014;121:1143-57.
20. Fortin D. The Blood-Brain Barrier: Its Influence in the Treatment of Brain Tumors Metastases. Current Cancer Drug Targets. 2012;12(3):247-59.
21. Engelhardt S, et al. Cell-specific blood-brain barrier regulation in health and disease: a focus on hypoxia. British Journal of Pharmacology. 2014;171(5):1210-30.
22. Dubois LG, et al. Gliomas and the vascular fragility of the blood brain barrier. Frontiers in Cellular Neuroscience. 2014;8:418.
23. Fidler IJ. The Biology of Brain Metastasis. The Cancer Journal. 2015;21(4):284-93.

24. Sofroniew MV, Vinters HV. Astrocytes: biology and pathology. Acta Neuropathologica. 2009;119(1):7-35.
25. Ahluwalia MS, et al. Brain metastasis and treatment. F1000Prime Reports. 2014;6:114.
26. Gimsa U, et al. Immune Privilege as an Intrinsic CNS Property: Astrocytes Protect the CNS against T-Cell-Mediated Neuroinflammation. Mediators of Inflammation. 2013;2013:1-11.
27. Faraji AH, Wipf P. Nanoparticles in cellular drug delivery. Bioorganic & Medicinal Chemistry. 2009;17(8):2950-62.
28. Fellner S, et al. Transport of paclitaxel (Taxol) across the blood-brain barrier in vitro and in vivo. Journal of Clinical Investigation. 2002;110(9):1309-18.
29. Fu Y, et al. Bevacizumab plus chemotherapy versus chemotherapy alone for preventing brain metastasis derived from advanced lung cancer. Journal of Chemotherapy. 2016; 28(3):218-24.
30. Zhang RD, et al. Differential permeability of the blood-brain barrier in experimental brain metastases produced by human neoplasms implanted into nude mice. The American journal of pathology. 1992;141(5):1115-24.
31. Miles FL, et al. Stepping out of the flow: capillary extravasation in cancer metastasis. Clinical & Experimental Metastasis. 2007;25(4):305-24.
32. Zhao L-n, et al. Vascular Endothelial Growth Factor Increases Permeability of the Blood–Tumor Barrier via Caveolae-Mediated Transcellular Pathway. Journal of Molecular Neuroscience. 2010;44(2):122-9.

Figures

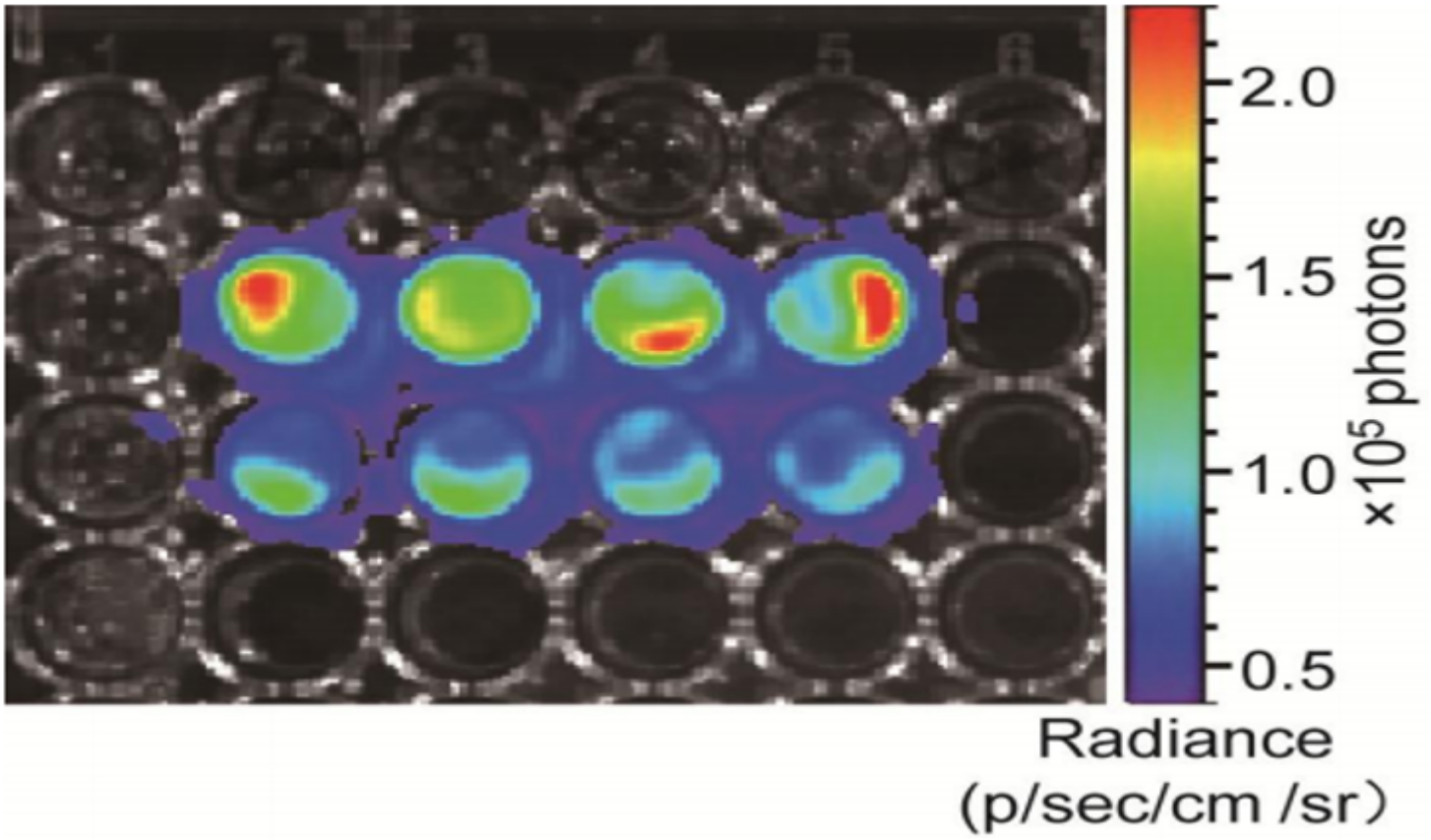

Figure 1

The cell fluorescence intensity of the Lewis cell line transfected with the Luc reporter gene.

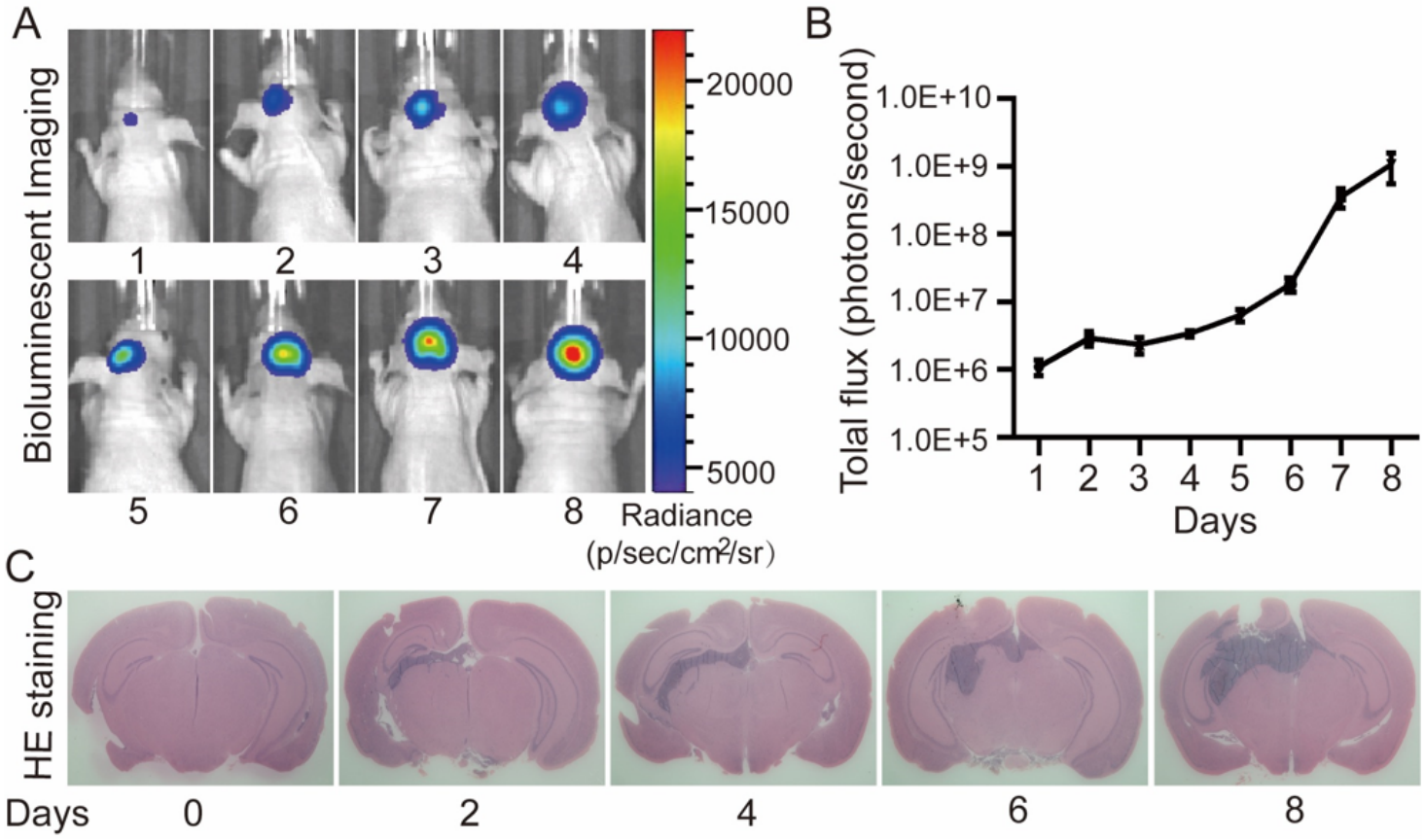

Figure 2

A and B: Tumor fluorescence intensity detected by a small animal imaging system. C: H&E staining of brain sections of tumor-bearing mice. Data are expressed as x±SEM, n=5.

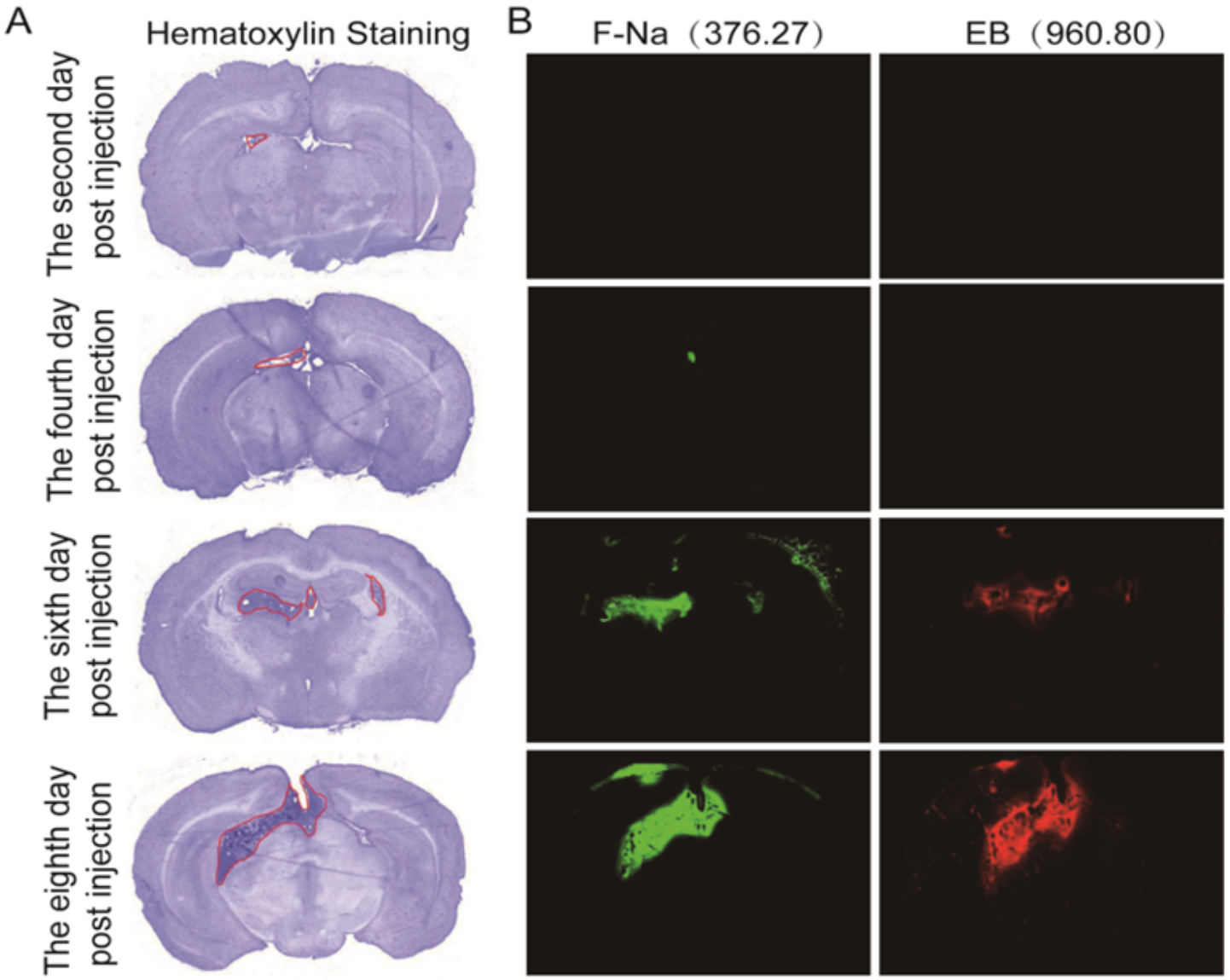

Figure 3

A: Hematoxylin staining showed that the volume of brain metastases increased gradually after implantation of Lewis cells. B: Fluorescent dye perfusion results showed that F-Na, which is a small molecule, permeation appeared on the 4th day after implantation of Lewis cells, while EB, with a relatively large molecular weight, could be detected on the 6th day. The fluorescence intensity increased over time after implantation of Lewis cells. Green indicates F-Na, and red indicates EB.

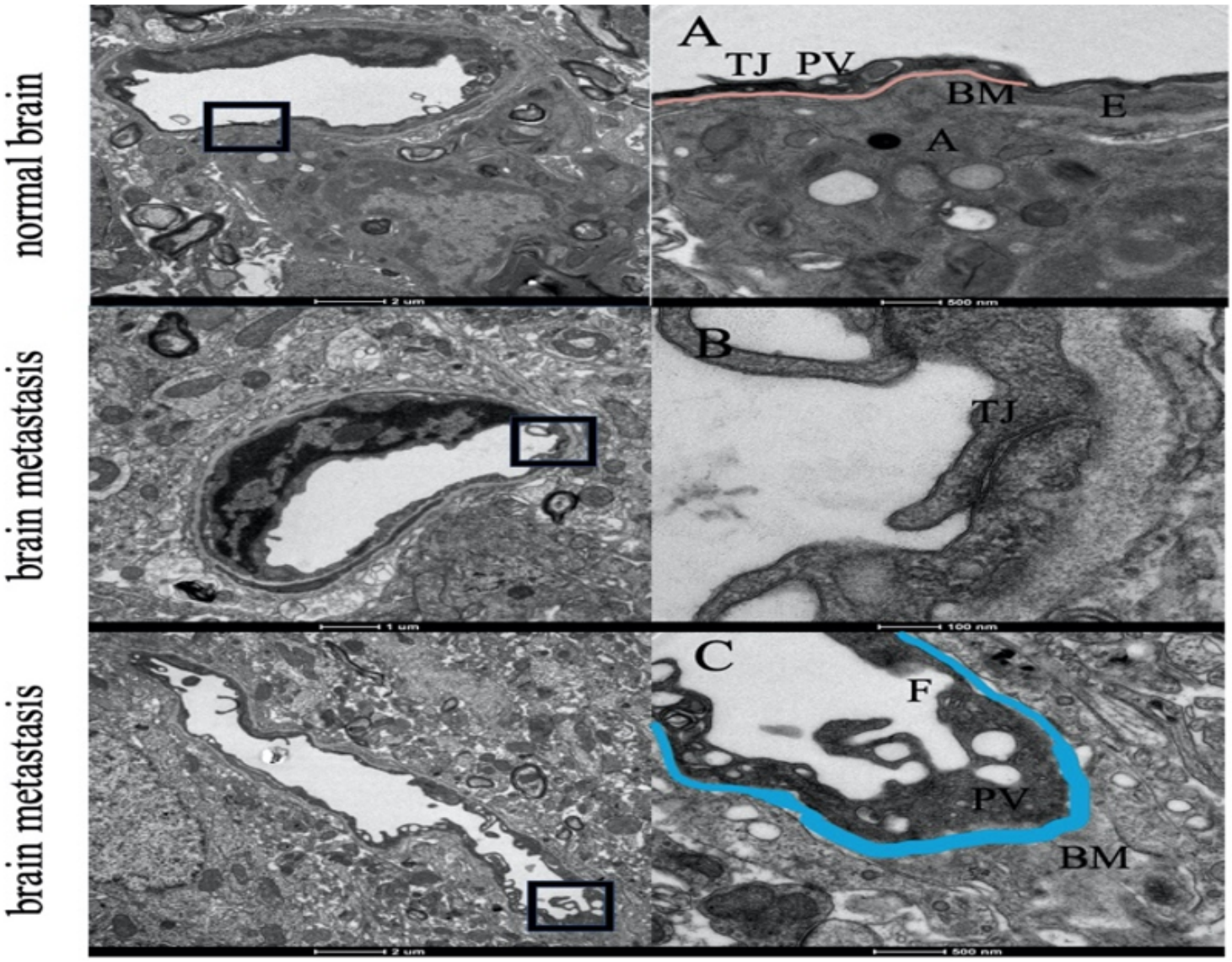

Figure 4

The ultrastructure of the BBB in brain metastases was observed by transmission electron microscopy. A shows an enlarged image of a normal BBB, while B and C show an enlarged image of the BBB of brain metastases. Panel E shows endothelial cells, A indicates an astrocyte, TJ indicates a tight junction, BM indicates the basement membrane, F indicates the fenestra of an endothelial cell, and PV indicates a pinocytotic vesicle.

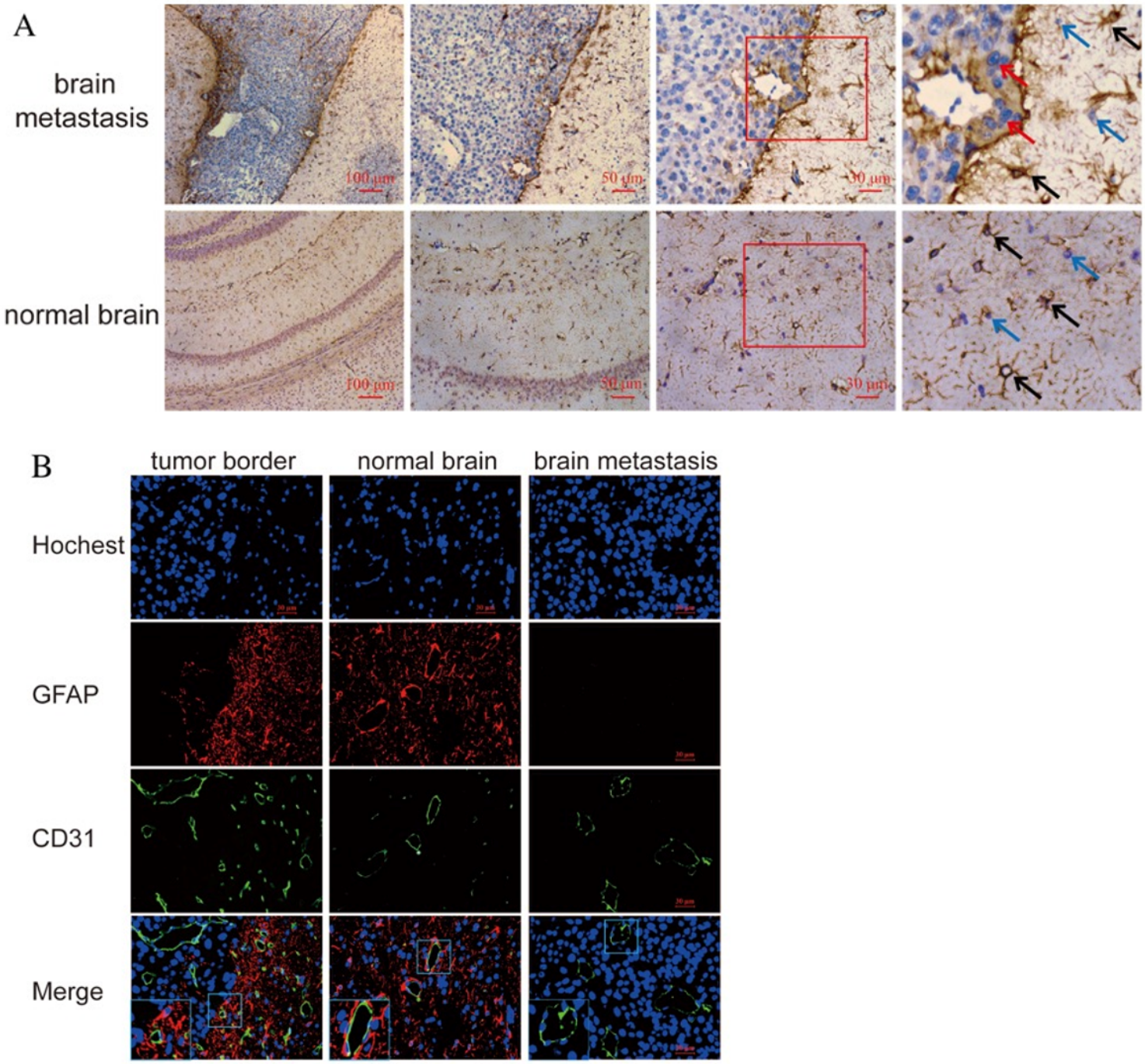

Figure 5

IHC and IF analyses showed that astrocytes were recruited at the borders of tumors and were surrounded by blood vessels in healthy brain tissue, but no astrocytes were found in metastases. The right column of Panel A and the lower left rectangular box of Panel B show enlarged parts of the image; the black arrow indicates an astrocyte, the blue arrow indicates brain tissue, and the red arrow indicates the tumor.

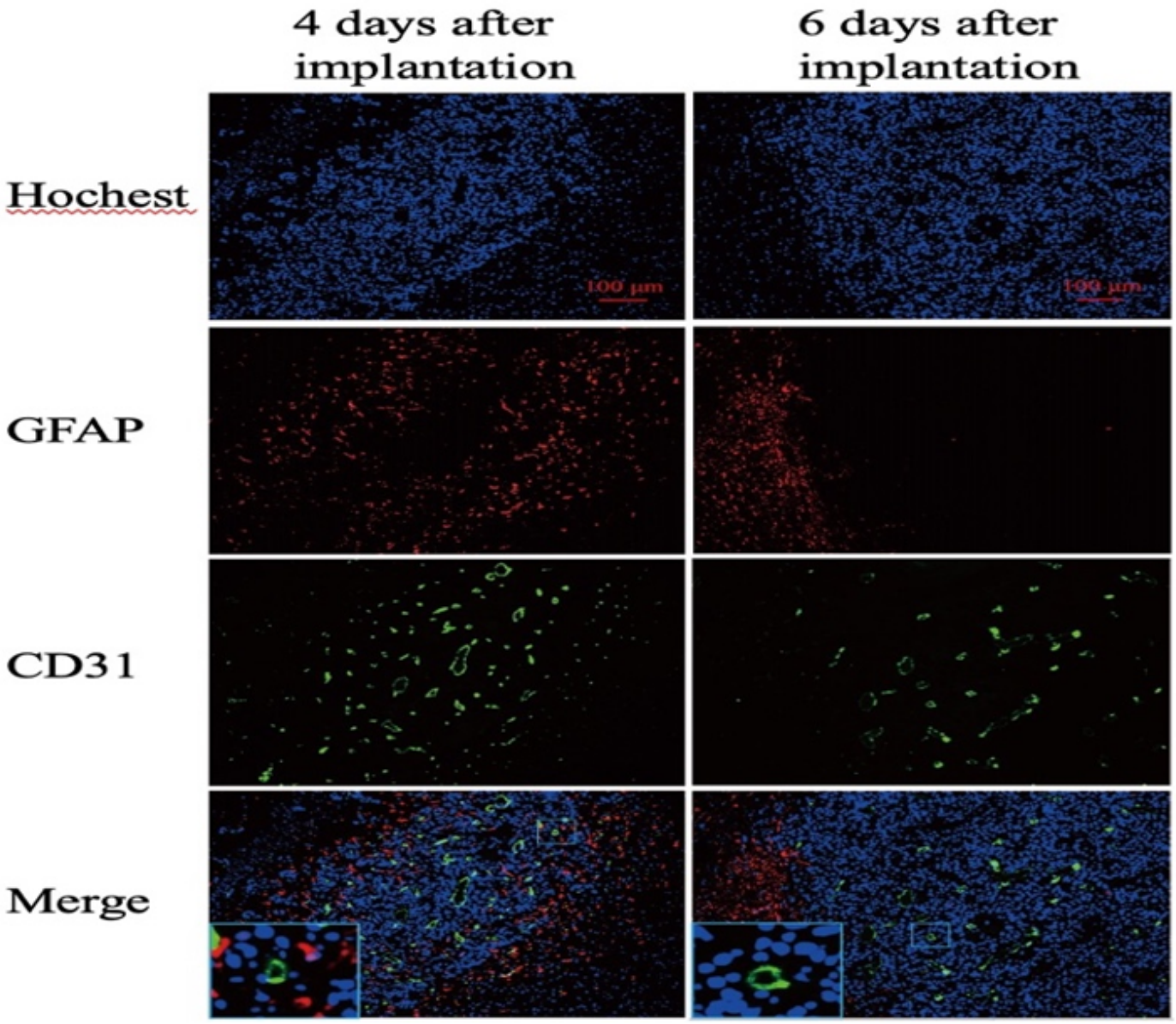

Figure 6

Astrocyte recruitment is visible around brain metastases and in smaller metastases (4 days after implantation). The lower left rectangular box shows an enlarged portion of the image.

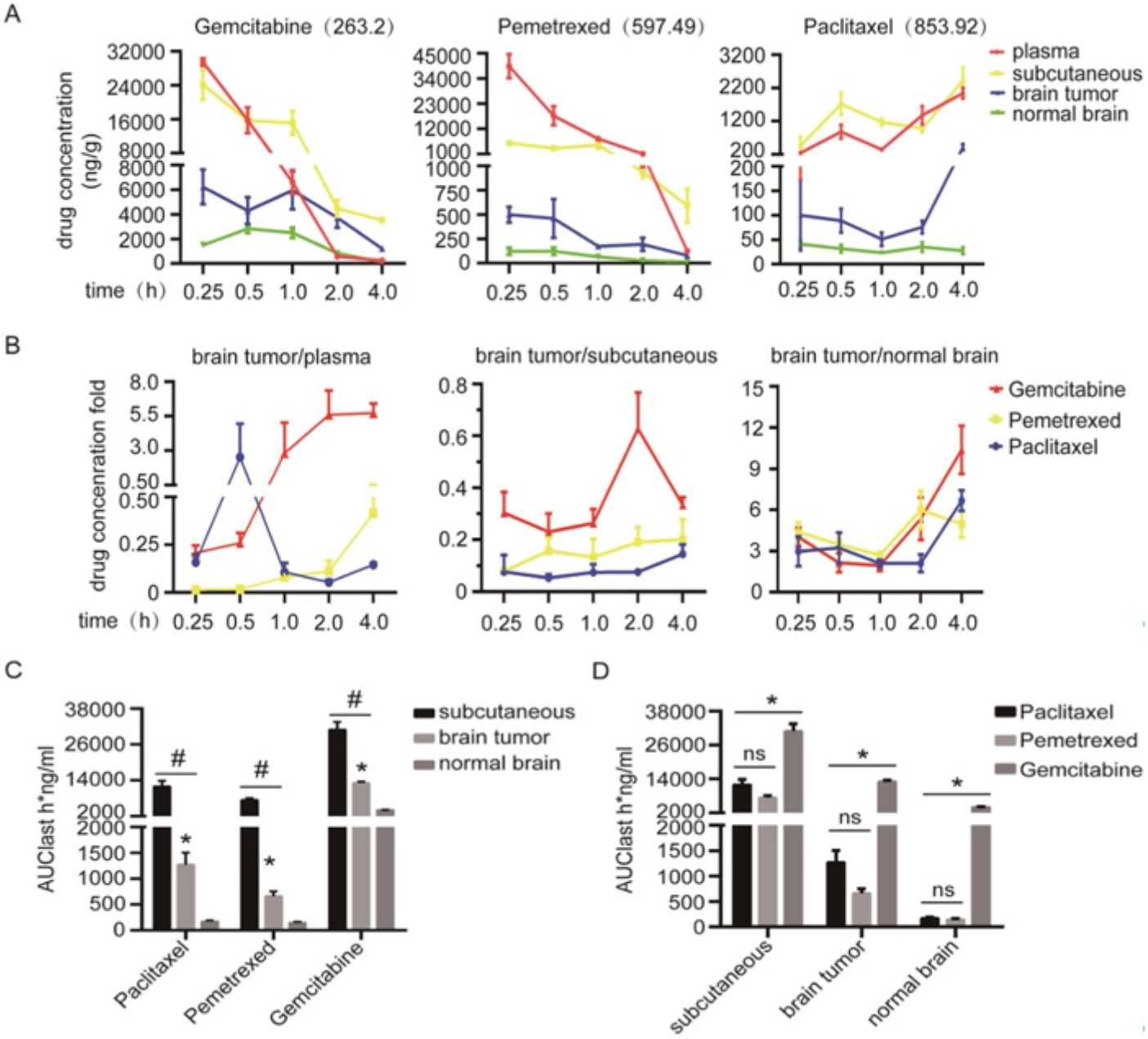

Figure 7

A and B: LC-MS/MS was used to detect the distribution of drugs in different tissues. The three types of chemotherapeutic drugs were more concentrated in brain tumors than in normal brain tissues but were less concentrated in peripheral tumors than in normal brain tissues. C and D: The area under the concentration-time curve of three chemotherapeutic drugs (AUClast). C* indicates a comparison with normal brain tissues, P<0.05; # indicates a comparison with subcutaneous tumors, P<0.05; D* indicates a comparison with pemetrexed and paclitaxel, P□0.05; (x±SEM, n=4).